Journal of the Korean Ceramic Society
Vol. 55, No. 2, pp. 178~184, 2018.

https://doi.org/10.4191/kcers.2018.55.2.11

Study on High-Temperature Oxidation Behaviors of Plasma-Sprayed TiB_2-Co Composite Coatings

Milad Fadavi†, Amin Rabiei Baboukani, Hossein Edris, and Mahdi Salehi

Department of Materials Engineering, Isfahan University of Technology, Isfahan 84156-83111, Iran

(Received February 12, 2018; Revised March 9, 2018; Accepted March 13, 2018)

ABSTRACT

In the present study, TiB_2-Co composite coatings were thermally sprayed onto the surface of a 304 stainless steel substrate using an atmospheric plasma spray (APS). The phase analysis of the powders and plasma-sprayed coatings was performed using X-ray diffractometry analysis. The microstructures of the coatings were studied by a scanning electron microscope (SEM). The average particle size and flowability of the feedstocks were also measured. Both TiB_2-32Co and TiB_2-45Co (wt.%) coatings possessed typical dense lamellar structures and high-quality adhesion to the substrate. The oxidation behaviors of the coatings were studied at 900 °C in an atmospheric environment. In addition, the cross-sectional images of the oxidized coatings were analyzed by SEM. A thin and well-adhered layer was formed on the surface of both TiB_2-Co coatings, confirming satisfactory high-temperature oxidation resistance. The kinetic curves corresponding to the isothermal oxidation of the coatings illustrated a short transient stage from rapid to slow oxidation during the early portion of the oxidation experiment.

Key words : TiB_2, Cermet Coating, Thermal Spray, Oxidation, Composite

1. Introduction

Ultrahigh-temperature ceramics (UHTCs) are a group of ceramics that possess very high melting points (above 3000°C). Transition-metal borides and carbides of groups V and IV are both referred to as UHTCs.[1,2] Among the transition-metal borides, TiB_2 coatings are utilized to extend the service lifetimes of industrial tools because of their high hardness, wear resistance, and high-temperature stability. Recently, cermet coatings, which have the toughness of metals and hardness of ceramics, have received considerable attention from researchers. These coatings have been developed with low porosity and good wetting between the ceramic phases and metallic binders.[3-8]

Advanced thermal spraying processes such as plasma spray and high-velocity oxy-fuel (HVOF) are typically used to deposit coatings onto the surfaces of engineering materials to enhance their high-temperature oxidation resistance. HVOF coatings have several advantages, including better morphology, greater adhesion, and lower porosity. However, this method is not favorable for preparing ultrahigh-temperature coatings, such as TiB_2 composite coatings, because of the extremely high melting points of UTHCs. The atmospheric plasma spraying (APS) method is more suitable for preparing coatings from hard ceramic powders with high melting points.

The oxidation resistivity, cracking resistivity, and limited diffusion between the substrate and coating are the most critical parameters in determining the coating efficiency for high-temperature applications.[9-12]

The research on materials for applications at elevated temperatures has attracted significant research attention.[1,2,13,14]

The demand for the improvement of high-temperature material performance inspired more extensive studies on this topic. The alloy of tungsten carbide-cobalt (WC-Co) is commonly used as a commercial coating material because of its attractive properties such as hardness and wear resistance.[15] However, the lack of high-temperature stability makes this alloy less favorable for coating applications.

Some studies have investigated the coating of steel with titanium carbide (TiC).[16-18] However, TiC coatings suffer from some disadvantages including the formation of highly porous coatings induced by the release of CO_2 gas during the oxidation process at elevated temperatures. The porosity provides paths for oxygen diffusion, leading to increased oxidation, which is not favorable. On the other hand, for the UHTC borides, it has been reported that the formation of boron trioxide (B_2O_3) can seal oxide cracks and pores because B_2O_3 melts at approximately 450°C. Therefore, it decreases oxygen transportation into the oxide interface, leading to less oxidation. Hence, at high temperature, TiB_2-based coatings have been considered among the most promising coating materials.[19,20]

Several studies have analyzed the protection of TiB_2 containing coatings at elevated temperatures. Some experiments illustrated that TiB_2 particles would increase the oxidation rate,[21] while others showed oxidation resistance

†Corresponding author : Milad Fadavi
E-mail : miladfadavi85@gmail.com
Tel : +98-9131033226

improvements by increasing the TiB_2 contents.[22] Lotfi *et al.* studied the high-temperature oxidation behaviors of HVOF-sprayed TiB_2 cermet coatings and reported that the HVOF-sprayed NiCr-TiB_2 coating showed high oxidation resistance and the predominant oxide scale phase of rutile (TiO_2).[22]

In the present work, TiB_2-32Co and TiB_2-45Co (wt.%) composite coatings have been successfully prepared by APS from powders that were ball-milled. The objective of this study was to investigate the cyclic oxidation behaviors of plasma-sprayed TiB_2-Co composite coatings in comparison to those of uncoated samples and commercial NiCr-Cr_2C_3 coatings to determine the oxidation resistances of these composites.

2. Experimental procedure

2.1. Primary materials

As the starting materials, TiB_2 and Co powders (Alfa Aesar) with purities of 99% were used. The TiB_2 powders had irregular morphologies with the particle size distribution of 40 - 100 μm, while the Co particle size was less than 10 μm. TiB_2 and Co powders were mixed together and ball-milled for 5 h in a high-energy planetary ball mill (AsanTech PA34500), at room temperature, under an Ar atmosphere. For comparison in oxidation experiments, a gas-atomized NiCr-Cr_2C_3 alloy (Metco™ 5241) was thermally sprayed onto the samples. A bond layer of Ni-Al coating was selected to accommodate the thermal expansion coefficient mismatch between the coating and substrate. ISI 304 stainless steel (composition: base of Fe, 0.08% C, 19% Cr, 11% Ni, < 2% Mn, < 1% Si, < 0.045% P, < 0.03% S) was used as the substrate. Disk-shaped samples (5 cm in diameter and 5 mm in thickness) were polished using 320-grit SiC abrasive paper and degreased by acetone before the deposition of the coatings.

2.2. Coating processing

The spray-drying technique was used to increase the flow rate of the feedstock powder. This process was performed in an experimental spray-dryer machine (Isfahan University of Technology, Isfahan, Iran, P3500). The spray-dry process is necessary for feedstock powders because ball-milled powders have low flowability and non-spherical morphology.

For this purpose, the composite powders produced in the ball-mill process were added to a solution of distilled water (DI water) and polyvinyl alcohol (PVA). The solution was stirred using a mechanical mixer until it formed a homogenous slurry. The powder to DI water and PVA to powder ratios were 1 : 10 and 1 : 100, respectively. The homogenous slurry was poured into the spray-dryer machine. The parameters of spray drying are listed in Table 1.

Table 1. The Parameters of Spray-Drying Process

Parameters	Values
Temperature (°C)	140
Rotation speed (rpm)	7200
Feeding rate ($mL \cdot min^{-1}$)	16.6

The coating process was carried out using a PS50-PC torch (PACO, Isfahan, Iran) on the surface of an ISI 304 stainless steel plate. The parameters of the thermal spray process are given in Table 2.

2.3. Oxidation experiments

In order to investigate the oxidation behaviors of the coatings, the cyclic oxidation of the prepared coatings was carried out in a conventional furnace under air atmosphere at 900°C for 40 h with the heating rate of 5°C/min. There were three samples for each composition for more precise experimental measurements. The sample dimensions for the oxidation tests were 10 × 10 × 5 mm. Before the oxidation tests, all of the coatings were ground and polished in order to achieve smooth surfaces with similar coating thicknesses. Every 5 h, the samples were taken out of the furnace and exposed to air for cooling. The samples were weighed after cooling using an electronic scale with decimal precision to four places.

2.4. Characterization

The phases and the microstructures of the powders and coatings were analyzed by X-ray diffraction (XRD, Philips X'PERT MPD diffractometer using filtered Cu Kα radiation (α = 0.1542 nm)) and a scanning electron microscope (SEM, Philips XL30). The average particle sizes, coating thicknesses, and porosities were estimated from SEM images using CLEMEX software version 4.0. The flow rate of the feedstock powder was measured according to the ASTM B 213-03 standard. In order to evaluate the microhardness values of the cross-sections of the coatings, a Vickers indenter was employed at the load of 100 g and the dwell time of 10 s five times for each coating and the average of all measurements was reported. The surface roughness values of the coatings were measured by a portable surface measurement tester (Mitutoyo SJ-210). The average of five measurements for each sample was calculated and reported as the roughness value.

Table 2. Thermal Spray Parameters Used for the Preparation of TiB_2-Co Coatings

Coating	Parameter				
	Current (A)	Voltage (V)	Powder feed rate ($g \cdot min^{-1}$)	Carrier gas flow Ar (SLPM)	Spray distance (mm)
TiB_2-Co	550	30	28 - 30	4	100

3. Results and Discussion

3.1. XRD analysis

The XRD patterns of as-sprayed coatings are presented in Fig. 1. According to the XRD results, the coating surface mainly consists of TiB_2 and $CoTiO_3$ along with a small amount of CoO. Because the temperature of the plasma jet is extremely high during the spraying, oxidation of Co is inevitable. In addition, a reaction between Co and Ti may occur to form the $CoTiO_3$ phase. The negligible amount of oxides formed in the coating confirms that the parameters used for the spraying process are selected reasonably.[23]

The XRD analysis (Fig. 2) of the oxidized surfaces of the coatings reveals that, after the oxidation experiment, the coatings are comprised of TiO_2 and B_2O_3 at 900°C. TiO_2 is the main oxide phase, and B_2O_3 is the second phase. Moreover, a small amount of $CoTiO_3$ is observed in the composite coatings. Thermodynamically, the presence of TiO_2 as the predominant phase is evident. The enthalpy of formation of TiO_2 (–944 kJ/mol) is much lower than that for other oxides so that this composition is more stable and can form easier.

Koh *et al.*[24] studied the high-temperature oxidation behavior of the TiB_2 compound and reported that, after the oxidation test of the TiB_2 sample in air at 800°C, intense TiO_2 and B_2O_3 peaks and a weak TiB_2 peak were observed in the XRD pattern. B_2O_3 can be amorphous or crystalline.[25-27] However, in our study, an intense B_2O_3 peak was observed.

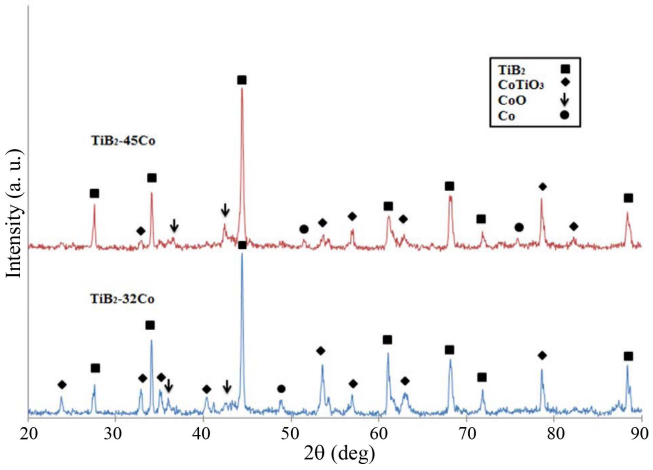

Fig. 1. XRD patterns of as-sprayed coatings.

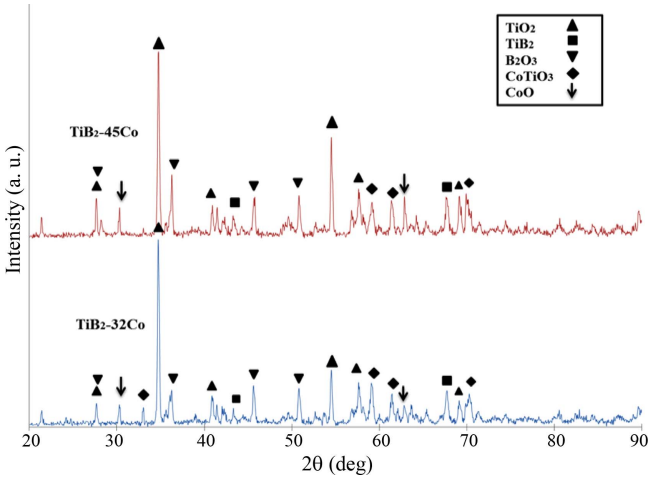

Fig. 2. XRD patterns of oxidized surfaces of TiB_2-Co coatings.

3.2. Oxidation behaviors of coatings

The oxidation behaviors of the TiB_2-Co cermet coatings were characterized by measuring the mass change per surface area.[28] A similar approach has been used to investigate the oxidation impact via the weight changes of other ceramic materials.[29,30] Fig. 3(a) shows the mass gain per unit area versus oxidation time of the coatings after oxidation experiment at 900°C for 40 h. Mass gain occurs with increases in the time, and the oxidation rate is high during the early hours of oxidation. However, because of the formation of the protective oxide layer on the coating surface, the oxidation rate decreases sharply, especially for the TiB_2-Co cermet coatings, and a stable oxidation stage is obvious at the end of the test. Minor spallation occurred on the surfaces of the coatings in the experiments because of the presence of TiB_2 as a stable compound. Moreover, the oxidation rates in the coated samples are noticeably smaller than that in the substrate. Even for NiCr-Cr_2C_3, which is a commercial coating for high-temperature usage in industry, weaker resistance to oxidation at 900°C is observed.[31] All mass gain diagrams indicate a non-linear behavior. The oxidation rate

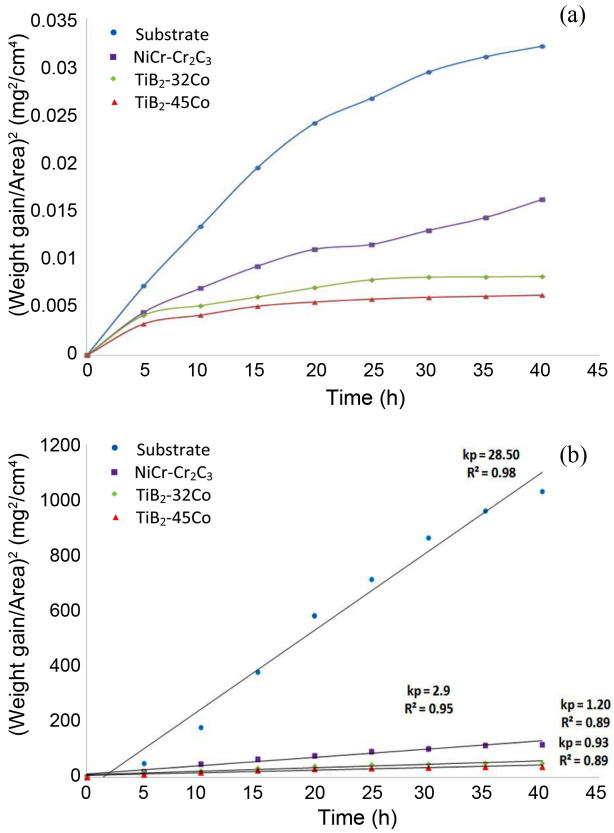

Fig. 3. Specific mass gain versus oxidation time for the substrate and the coatings at 900°C.

is parabolic at this temperature, and can be described by equation (1).[32]

$$\left(\frac{\Delta m}{S}\right)^2 = k_p t + c \quad (1)$$

where Δm is the mass change, t is the oxidation time, and k_p and c represent the oxidation kinetic constants.[33] Fig. 3(b) shows the kinetic curves of the isothermal oxidation of the coatings and the substrate at 900°C. In order to determine if the kinetic trend is parabolic, plotting the square of the weight gain per unit area versus time is essential. The oxidation kinetics follows the parabolic rate equation when most of the data points fit into a straight line. The mass gain curve (Fig. 4(b)) indicates a diffusion- controlled kinetics. The parabolic rate constant, k_p, is determined as 1.20 and 0.93 $mg^2/(cm^4 \cdot h)$ for TiB_2-32Co and TiB_2-45Co coatings, respectively. This value is comparable to those of TiB_2-based ceramics.[34]

The oxidation resistance of the prepared coatings is higher than that of WC-Co coatings, which were oxidized in the temperature range of 400 - 500°C.[35-37] It has been proved that the WC-Co coatings in the best condition can present good resistance at 800°C for only 3 h.[38]

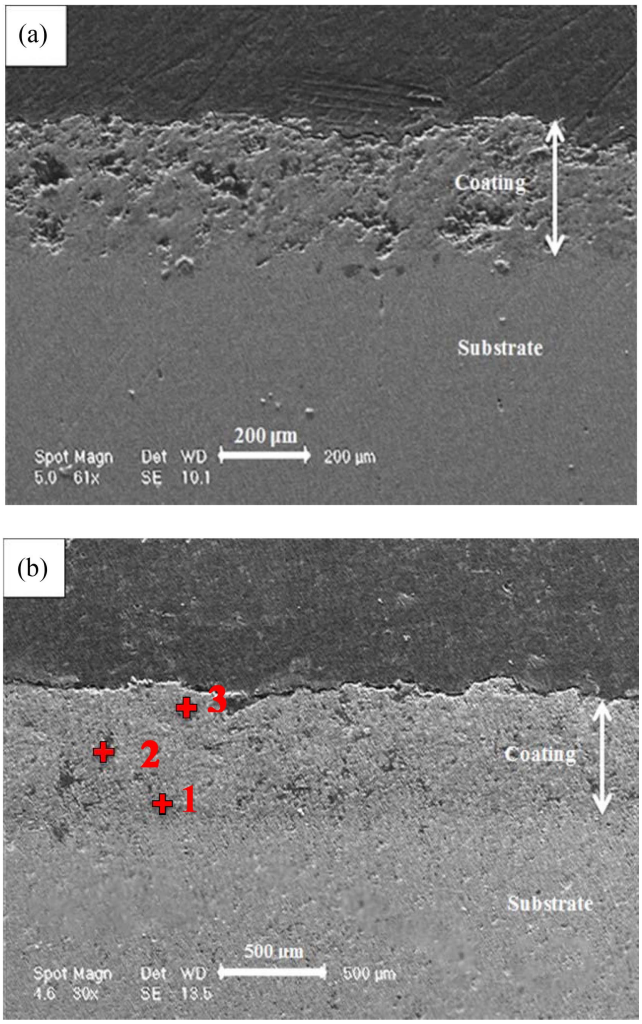

Fig. 4. Cross-sectional SEM images of as-sprayed coatings (a) TiB_2-32Co (b) TiB_2-45Co.

3.3. SEM analysis of the as-sprayed and oxidized coatings

Figure 4 shows the cross-sectional SEM images of the as-sprayed coatings. All the coatings have layered morphologies due to the deposition of both molten and semi-molten droplets. The coatings are relatively dense and well bonded to the steel substrate. A Ni-Al bond coat was used for increasing the adhesion of the coatings and the interfaces between the coatings and substrate are free of any significant cracks or detachments. Because the TiB_2 particles in the coatings were not uniform in size, some of these particles were easily pulled out during the metallographic polishing process.[39] This would happen occasionally during the sample preparation of thermally sprayed cermet coatings.[40,41] Moreover, TiB_2-32Co (wt.%) shows relatively higher porosity in comparison with the TiB_2-45Co(Wt.%) coating, because of the higher volume percentage of TiB_2 in this coating. The properties of the composite coatings are listed in Table 3.

Figure 5 shows the SEM images of the cross-sections of the coatings oxidized at 900°C for 40 h. As can be seen in Fig. 5(a), a TiO_2 oxide layer with the thickness of approximately 20 µm is observed on the surface of the coating. As can be seen in Fig. 5, a mixed oxide layer beneath the TiO_2, which mainly consists of B_2O_3, seals the pores of the coating and protects the base layer from oxidation. This protective oxide layer decreases the oxidation rate at high temperature and creates the non-linear behavior in the mass gain diagram (Fig. 3).

3.4. EDS analysis

According to the energy-dispersive X-ray spectroscopy (EDS) analysis, as shown in Table 4, Ti and Co are the main elements in the TiB_2-45 Co coating. The presence of Ni at point 1 is related to the Ni-5%Al (wt.%) bond-coat. The analysis at point 2 illustrates that the region near the porous area is rich in O and B. This porosity may be the result of in-flight oxidation. In the APS process, because of the higher particle temperature and stronger gas mixing in the vicinity of the in-flight particles, the porosity of coatings is much greater than that of those in the HVOF process.[42] There are two aspects that play major roles in obtaining an excellent TiB_2-based cermet coating with superior mechanical properties. The first is to retain more TiB_2 particles in the coating;

Table 3. Characteristics of As-Sprayed Coatings

Characteristics	Coatings	
	TiB_2-32%Co	TiB_2-45%Co
Thickness (µm)	295 ± 25	406 ± 35
Surface roughness, R_a (µm)	14 ± 3	12 ± 2
Porosity (%)	12.3 ± 2	9.1 ± 2
Microhardness (H_v)	906 ± 34	878 ± 55

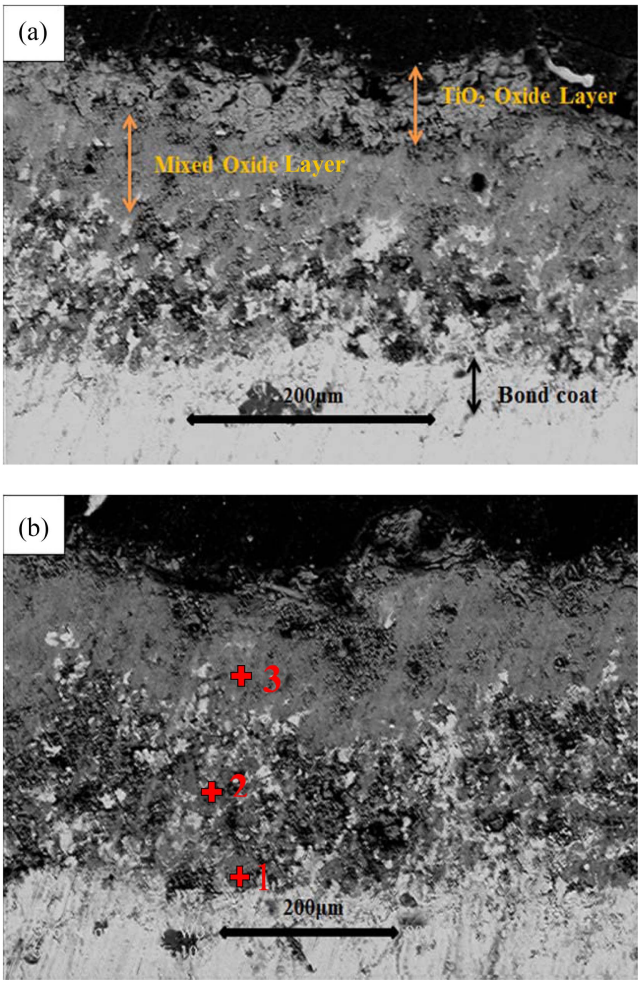

Fig. 5. Cross-sections of backscattered electron images of oxidized coatings (a) TiB_2-32Co (b) TiB_2-45Co.

Table 4. EDS Analysis Results (at.%) of the TiB_2-45Co Coating

Point#	Ti	Co	Ni	B	O
1	29.91	13.92	51.46	4.71	0.00
2	42.23	38.76	N/A	7.16	11.85
3	50.19	41.27	N/A	5.84	2.70

Table 5. EDS Analysis Results (at.%) of the Oxidized TiB_2-45Co Coating

Point#	Ti	Co	Ni	B	O
1	24.70	8.86	49.35	13.79	3.50
2	42.66	19.63	N/A	7.90	30.01
3	39.63	13.18	N/A	1.38	45.80

the second is to suppress the reaction between TiB_2 and the binder in order to avoid the formation of brittle phases. Appropriate feedstock parameters such as TiB_2 particle size, binder phase, and powder structure, and the use of the HVOF technique with a low flame temperature can significantly increase the quality of the coatings.[43]

It can be seen from Table 5 that, near the surface of the coating, Ti and O are prominent in the EDS analysis. The low content of oxides in point 1 illustrates that the TiB_2-45 wt.% Co coating has good oxidation resistance.

It should be also mentioned that the differences between thickness, roughness, porosity, and hardness between the two coated materials might be due to the amounts of metallic content (Co) or binder. For example, more binder would lead to the formation of a less porous coating with lower hardness.

4. Conclusions

The following conclusions could be drawn based on the experimental results obtained in this study:

1) The APS thermally sprayed TiB_2-Co coatings exhibited high oxidation resistance. The oxide layer consisted of a thin layer of TiO_2 and the adherent mixed oxide layer mainly contained B_2O_3 at 900°C, with no signs of delamination or cracking.

2) The microstructure of TiB_2-45Co had lower porosity than TiB_2-32Co, so the oxidation resistance of TiB_2-45Co was better than that of TiB_2-32Co.

3) The oxidation kinetics of the coating at 900ºC followed a parabolic rate law. The oxide layer was thin and had good adhesion to the coating. The coatings showed satisfactory high-temperature oxidation resistance.

4) For almost all coatings, a parabolic rate law was observed in oxidation kinetics, but the TiB_2-Co composite coatings illustrated a significantly smaller oxidation rate than the bare substrate and even the commercial NiCr-Cr_2C_3 coating.

REFERENCES

1. W. G. Fahrenholtz, G. E. Hilmas, I. G. Talmy, and J. A. Zaykoski, "Refractory Diborides of Zirconium and Hafnium," *J. Am. Ceram. Soc.,* **90** [5] 1347-64 (2007).
2. P. Foroughi, C. Zhang, A. Agarwal, and Z. Cheng, "Controlling Phase Separation of $Ta_xHf_{1-x}C$ Solid Solution Nanopowders during Carbothermal Reduction Synthesis," *J. Am. Ceram. Soc.,* **100** [11] 5056-65 (2017).
3. F. Kikkawa, H. Tamura, and K.-I. Kondo, "Ti-B-C Composite Coating Produced by Electrothermally Exploded Powder-Spray Technique," *J. Therm. Spray Technol.,* **15** [1] 92-6 (2006).
4. B. Du, S. R. Paital, and N. B. Dahotre, "Phase Constituents and Microstructure of Laser Synthesized TiB_2-TiC Reinforced Composite Coating on Steel," *Scr. Mater.,* **59** [10] 1147-50 (2008).
5. V. N. Zhitomirsky, S. Wald, M. Factor, L. Rabani, D. Zoler, S. Cuperman, C. Bruma, and I. Roman, "WC-Co Coatings Deposited by the Electro-Thermal Chemical Spray Method," *Surf. Coat. Technol.,* **132** [1] 80-8 (2000).
6. Q. Yang, T. Senda, and A. Ohmori, "Effect of Carbide Grain Size on Microstructure and Sliding Wear Behavior of HVOF-Sprayed WC-12% Co Coatings," *Wear,* **254** [1] 23-

34 (2003).
7. J. M. Guilemany, J. M. Miguel, S. Vizcaino, and F. Climent, "Role of Three-Body Abrasion Wear in the Sliding Wear Behaviour of WC-Co Coatings Obtained by Thermal Spraying," *Surf. Coat. Technol.,* **140** [2] 141-46 (2001).
8. H. Hassannejad, M. Moghaddasi, E. Saebnoori, and A. R. Baboukani, "Microstructure, Deposition Mechanism and Corrosion Behavior of Nanostructured Cerium Oxide Conversion Coating Modified with Chitosan on AA2024 Aluminum Alloy," *J. Alloys Compd.,* **725** 968-75 (2017).
9. S. Kumar, D. Mudgal, S. Singh, and S. Prakash, "Cyclic Oxidation Behavior of Bare and Cr_3C_2-25 (NiCr) Coated Super Alloy at Elevated Temperature," *Adv. Mater. Lett.,* **4** [10] 754-61 (2013).
10. C. T. Sims, N. S. Stolloff, and W. C. Hagel, Superalloys II; pp. 359, Wiley, New York, 1987.
11. A. R. Baboukani, E. Sharifi, S. Akhavan, and A. Saatchi, "Co Complexes as a Corrosion Inhibitor for 316 L Stainless Steel in H_2SO_4 Solution," *J. Mater. Sci. Chem. Eng.,* **4** [9] 28-35 (2016).
12. M. Mohammadi, S. Javadpoura, A. Kobayashi, K. Shirvani, J. A. Jahromi, and I. Khakpour, "Cyclic Oxidation Behavior of CoNiCrAlY Coatings Produced by LVPS and HVOF Processes," *Trans. JWRI,* **40** [1] 53-8 (2011).
13. Z. Cheng, P. Foroughi, and A. Behrens, "Synthesis of Nanocrystalline TaC Powders via Single-Step High Temperature Spray Pyrolysis from Solution Precursors," *Ceram. Int.,* **43** [3] 3431-34 (2017).
14. A. R. Baboukani, A. Saatchi, and R, Ebrahimi-Kahrizsangi, "Solid State Displacement Reaction Between Ni and CuO As a High Temperature Composite, The 3rd International," pp. 71-73. in *The 3rd International Conference on Composites: Characterization, Fabrication and Application (CCFA-3) Tehran*. Iran, 2012.
15. S. M. Nahvi and M. Jafari, "Microstructural and Mechanical Properties of Advanced HVOF-Sprayed WC-based Cermet Coatings," *Surf. Coat. Technol.,* **286** 95-102 (2016).
16. C. K. Sahoo and M. Masanta, "Microstructure and Mechanical Properties of TiC-Ni Coating on AISI304 Steel Produced by TIG Cladding Process," *J. Mater. Process. Technol.,* **240** 126-37 (2017).
17. F. Saba, E. Kabiri, J. V. Khaki, and M. H. Sabzevar, "Fabrication of Nanocrystalline TiC Coating on AISI D2 Steel Substrate via High-Energy Mechanical Alloying of Ti and C," *Powder Technol.,* **288** 76-86 (2016).
18. S. J. Algodi, J. W. Murray, M. W. Fay, A. T. Clare, and P. D. Brown, "Electrical Discharge Coating of Nanostructured TiC-Fe Cermets on 304 Stainless Steel," *Surf. Coat. Technol.,* **307** 639-49 (2016).
19. R. Naslain, A. Guette, F. Rebillat, S. Le Gallet, F. Lamouroux, L. Filipuzzi, and C. Louchet, "Oxidation Mechanisms and Kinetics of SiC-Matrix Composites and Their Constituents," *J. Mater. Sci.,* **39** [24] 7303-16 (2004).
20. X. Wang, H. Shun, C. Li, X. Wang, and D. Sun, "The Performances of TiB_2-Contained Iron-based Coatings at High Temperature," *Surf. Coat. Technol.,* **201** [6] 2500-4 (2006).
21. S. Hou, Z. Liu, D. Liu, and Y. Ma, "Oxidation Behavior of NiAl-TiB_2 Coatings Prepared by Electrothermal Explosion Ultrahigh Speed Spraying," *Phys. Procedia,* **32** 71-7 (2012).
22. B. Lotfi, "Elevated Temperature Oxidation Behavior of HVOF Sprayed TiB_2 Cermet Coating," *Trans. Nonferrous Met. Soc. China,* **20** [2] 243-47 (2010).
23. R. Agrawal, E. Adelowo, A. Baboukani, M. Villegas, A. Henriques, and C. Wang, "Electrostatic Spray Deposition-Based Manganese Oxide Films–From Pseudocapacitive Charge Storage Materials to Three-Dimensional Microelectrode Integrands," *Nanomaterials,* **7** [8] 198 (2017).
24. Y.-H. Koh, H.-W. Kim, and H. E. Kim, "Improvement in Oxidation Resistance of TiB_2 by Formation of Protective SiO_2 Layer on Surface," *J. Mater. Res.,* **16** [1] 132-37 (2001).
25. A. Agarwal, L. R. Katipelli, and N. B. Dahotre, "Elevated Temperature Oxidation of Laser Surface Engineered Composite Boride Coating on Steel," *Metall. Mater. Trans. A,* **31** [2] 461-73 (2000).
26. P. Foroughi and Z. Cheng, "Understanding the Morphological Variation in the Formation of B_4C via Carbothermal Reduction Reaction," *Ceram. Int.,* **42** [14] 15189-98 (2016).
27. P. Foroughi and Z. Cheng, "From Micron-Sized Particles to Nanoparticles and Nanobelts: Structural Non-Uniformity in the Synthesis of Boron Carbide by Carbothermal Reduction reaction," *pp. 51-62. in Advances in Ceramic Armor XI.* John Wiley & Sons, Inc., 364, 2015.
28. A. Navidinejad, E. SaebNoori, and A. R. Baboukani, "Mechanism Study and Parameter Optimization of A356 Aluminum Alloy Electrochemical Polishing," pp. 11-12. in *Proceedings of Iran International Aluminum Conference (IIAC2016).* Tehran, Iran.
29. S. Darvish, A. Karbasi, S. K. Saxena, and Y. Zhong, "Weight Loss Mechanism of $(La_{0.8}Sr_{0.2})_{0.98}MnO_{3\pm\delta}$ During Thermal Cycles," pp. 93-99. in *Mechanical Properties and Performance of Engineering Ceramics and Composites X.* John Wiley & Sons, Inc., 2015.
30. I. Khakpour, R. Soltani, and M. H. Sohi, "Microstructure and High Temperature Oxidation Behaviour of Zr-Doped Aluminide Coatings Fabricated on Nickel-based Super Alloy," *Procedia Mater. Sci.,* **11** 515-21 (2015).
31. S. Zolfaghari, A. R. Baboukani, A. Ashrafi, and A. Saatchi, "Investigation the Effects of Na_2MoO_4 as an Inhibitor on Electrochemical Corrosion Behavior of 316L Stainless Steel in LiBr Solution," *Zast. Mater.*, **59** [1] 108-16 (2018).
32. N. Birks, G. H. Meier, and F. S. Pettit, Introduction to the High Temperature Oxidation of Metals; Cambridge University Press, Cambridge, 2006.
33. V. A. Lavrenko, V. P. Konoval, A. D. Panasyuk, and A. P. Umanskii, "High-Temperatures Oxidation of AlN-$TiCrB_2$ Composites. I. Kinetics and Mechanism of Air Oxidation Up to 1600°C," *Powder Metall. Met. Ceram.,* **54** [7] 482-89 (2015).
34. C. Louro and A. Cavaleiro, "Oxidation Behaviour of W-N-M (M = Ni, Ti) Sputtered Films," *Surf. Coat. Technol.,* **74-75** 998-1004 (1995).
35. M. Jafari, M. H. Enayati, M. Salehi, S. M. Nahvi, and C. G. Park, "Comparison between Oxidation Kinetics of HVOF Sprayed WC–12Co and WC–10Co–4Cr Coatings," *Int. J. Refract. Met. Hard Mater.,* **41** 78-84 (2013).
36. H. L. de Villiers Lovelock, "Powder/Processing/Structure

Relationships in WC-Co Thermal Spray Coatings: A Review of the Published Literature," *J. Therm. Spray Technol.,* **7** [3] 357-73 (1998).
37. M. Peiravi, S. R. Mote, M. K. Mohanty, and J. Liu, "Bio-electrochemical Treatment of Acid Mine Drainage (AMD) from an Abandoned Coal Mine under Aerobic Condition," *J. Hazard. Mater.,* **333** 329-38 (2017).
38. M. Jafari, M. H. Enayati, M. Salehi, S. M. Nahvi, J. C. Han, and C. G. Park, "High Temperature Oxidation Behavior of Micro/Nanostructured WC-Co Coatings Deposited from Ni-Coated Powders Using High Velocity Oxygen Fuel Spraying," *Surf. Coat. Technol.,* **302** 426-37 (2016).
39. A. R. Baboukani, S. Akhavan, A. Saatchi, R. Ebrahimi-Kahrizsangi, and E. Saebnoori, "Mechanical Properties of AA2024 In the Presence of Al-Cu Intermetallic Surface Layer," pp. 28-31. *in Proceedings of Iran International Aluminum Conference (IIAC2016).*
40. J. F. Li and C. X. Ding, "Fractal Character of Circumferences of Polishing-Induced Pull Outs of Plasma Sprayed Cr_3C_2-NiCr Coatings," *Thin Solid Films,* **376** [1] 179-82 (2000).
41. Z. Khoshkhou, M. Torkghashghaei, and A. R. Baboukani, "Corrosion Inhibition of Henna Extract on Carbon Steel with Hybrid Coating TMSM-PMMA in HCL Solution," *Open J. Synth. Theory Appl.,* **7** [1] 1-16 (2018).
42. S. Deshpande, S. Sampath, and H. Zhang, "Mechanisms of Oxidation and its Role in Microstructural Evolution of Metallic Thermal Spray Coatings-Case Study for Ni-Al," *Surf. Coat. Technol.,* **200** [18] 5395-406 (2006).
43. J. R. Davis, "Handbook of Thermal Spray Technology;" ASM International, Ohio, 2004.